Journal of
Synchrotron Radiation

ISSN 0909-0495

Received 5 July 2010
Accepted 19 December 2010

On aberrations in saw-tooth refractive X-ray lenses and on their removal

Werner Jark

Sincotrone Trieste ScpA, SS 14 km 163.5, I-34012 Basovizza (TS), Italy.
E-mail: werner.jark@elettra.trieste.it

The X-ray lens, which is composed of opposing canted saw-tooth structures, originally assembled from cut-out pieces from long-playing records, is understood by recognizing that an incident plane X-ray wave will traverse a varying number of triangular prisms in them. The refraction will deflect any beam towards the prism tips and the variation of the deflection angle, which grows linearly with the number of traversed prisms, can result in X-ray focusing. The structure offers focusing flexibility by simply changing the taper angle. This report will discuss the aberrations arising in the saw-tooth structure in its simplest form with identical prisms. It is found that the saw-tooth structures in low-Z materials with focal length below 1 m provide less flux density in the focal spot than stacks of one-dimensionally focusing refractive lenses with identical transmission function. This is due to excessive aberrations in the regular structure, which are absent in stacks of concave lenses, and which limit the focusing to spot sizes of just submicrometre dimensions, as measured experimentally for some lenses. It will be shown that this limitation can be overcome by appropriately modifying the prism shape. Then the image size could be reduced by about an order of magnitude to the diffraction limit with competitive numbers even below 0.1 μm. Microfabrication techniques are identified as the appropriate means for producing the structures.

Keywords: X-ray optics; refractive lens; microfocus; diffraction-limited resolution.

1. Introduction

The most common optics for the focusing of light beams in the visible spectral range are transmission lenses, in which focusing is achieved by refraction at curved interfaces (see, for example, Born & Wolf, 1980). In the thin lens approximation and for spherical surfaces with radius of curvature R the focal length of a symmetric lens is given by

$$f_{\rm lens} = \frac{R}{2(n-1)}, \qquad (1)$$

where n is the refractive index of the lens material and $n_{\rm air} = 1$ is assumed for the environment in which it is operated. Here $R > 0$ describes convex lens surfaces, and a positive focal length $f > 0$ produces a real image downstream of the lens at image distances $p \geq f$.

Equation (1) is also applicable for hard X-rays. However, differently to the visible spectral range, the refractive index n of any material is slightly smaller than unity (James, 1967), and it is thus more conveniently written as $n = 1 - \delta$ with

$$\delta = \frac{N_{\rm A}}{2\pi} r_0 \lambda^2 \rho \frac{Z}{A}, \qquad (2)$$

where $N_{\rm A}$ is Avogadro's number, r_0 is the classical electron radius, ρ is the density, λ is the photon wavelength, and Z and A are the atomic number and the atomic mass, respectively. The lens equation (1) can then be written as

$$f_{\rm lens} = -R/2\delta. \qquad (3)$$

While for visible radiation the refractive index decrement δ is of the order of $\delta \simeq -0.5$, in the X-ray range $\delta < 10^{-5}$. The sign and magnitude of δ and the dispersion $\delta \propto \lambda^2$ now have important consequences. First of all the sign requires lenses with negative radius of curvature, *i.e.* concave surfaces, for the focusing of X-rays. Secondly the magnitude of δ requires radii of curvature in the micrometre range in order to realise lenses with focal length $f < 1$ m. Finally the strong dispersion, or chromaticity, makes a refractive X-ray lens a chromatic focusing device in which the focal length varies with photon energy. The first proposal by Tomie (1994) and the first tests at refractive X-ray lenses by Snigirev *et al.* (1996) regarded one-dimensionally focusing lenses obtained by using the material between a series of drilled holes. These objects were given the name compound refractive lens (abbreviated as CRL). State-of-the-art are now stacks of platelets with rotationally symmetric parabolic lenses for two-dimensional focusing (Lengeler *et al.*, 1999). By use of the latter lens shape the aberrations are minimized. Such a correction from purely spherical surfaces to parabolic surfaces is needed in order to

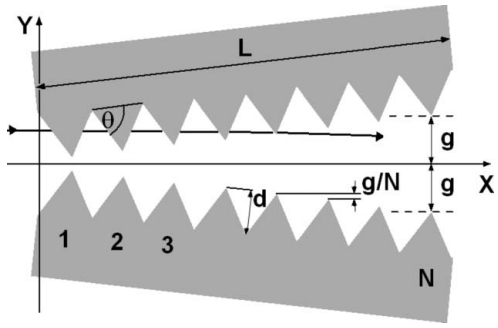

Figure 1
Scheme of the saw-tooth refractive lens (SRL) in the originally proposed orientation. The lens contains N teeth in a length L, has a largest opening of $2g$ for grooves of depth d and a prism angle of θ. The curved path for one ray is indicated. The x-axis is the symmetry axis, *i.e.* the optical axis, of the lens.

obtain spot sizes in the submicrometre range with lenses in low-Z material and with focal length $f < 1$ m. The continuous zooming of the focal length or the variation of the photon energy in a slit at fixed position, which the chromaticity of the lenses would permit, are not possible using lens stacks. Both operations modes are instead elegantly possible in a pair of prism arrays, as introduced by Cederström *et al.* (2000) and presented in Fig. 1, however, in only one dimension. Obviously a parallel beam passing through two facing and inclined prism arrays will be subject to a beam deflection which increases linearly with increasing off-axis distance. This focuses the transmitted X-rays and zooming can be achieved simply by changing the taper angle between the two grooved structures (Cederström *et al.*, 2000). As far as the material distribution is concerned orthogonally to the principal beam trajectory it is an advantageous parabolic profile composed of straight segments of equal height. For the zooming the height of the latter segments is varied continuously, which then changes the radius of curvature in the lens apex, while keeping a parabolic surface profile in one dimension. Bi-dimensional focusing then requires the operation of crossed lens pairs in a tandem configuration.

The first lens of this type was assembled by Cederström *et al.* (2000) from cut-out pieces from a long-playing record. The appearance of the lens led Dufresne *et al.* (2001) to dub it the alligator lens. Ultimately the description as saw-tooth refractive lens has become more common (Shastri *et al.*, 2007; Said & Shastri, 2010), and will be used here as well with the abbreviation SRL. The possibility of producing the grooved structures by milling, as originally done by Cederström *et al.* (2000), or by sawing, as more recently attempted by Said & Shastri (2010), *i.e.* by use of standard workshop tools, makes them a rather economic option for X-ray focusing. In the light of these two advantageous features, *i.e.* the zoomability and the ease of production, is it rather surprising that the literature presents only few studies related to their use in the ten years following their introduction. This may be due to the fact that the lens systems realised by Cederström *et al.* (2002*a*,*b*) and by Ribbing *et al.* (2003*a*,*b*) do not yet routinely provide the more desirable focus sizes far below 1 µm. However, it should be noted that Cederström *et al.* (2002*a*,*b*) optimized their objects primarily for use in mammography with larger spot sizes in combination with laboratory X-ray tubes, and they applied the microfocusing essentially for quality control. Now, for the purpose of mammography, which can very fruitfully use narrow X-ray lines provided by one-dimensional focusing, the lenses already almost present the expected performance as recently shown by Fredenberg *et al.* (2008).

This latter success has led to the study in more detail of the suitability of this lens concept for high-spatial-resolution focusing for projects involving synchrotron radiation sources. This report is thus addressing the question of how far the intrinsic parameters of the lens will limit the ultimately achievable resolution, and how far will they limit the spatial resolution in reported experiments. Finally, the possibility of eventually overcoming existing limitations is discussed. The theoretically possible ultimate performance is presented as well as a feasible structure for state-of-the-art technology.

2. Theoretical considerations

2.1. Boundary conditions

Cederström *et al.* (2000) derived the material distribution function in the saw-tooth refractive lens of Fig. 1 as

$$P_{\rm SRL}(y) = \frac{N}{g\tan\theta}\,y^2, \tag{4}$$

where N is the total number of prisms in the array, g is the half-gap at the lens termination and θ is the prism side-wall inclination at their bases.

This function is a parabola, to which one can then assign a nominal radius of curvature to be put to the centre of a now plane concave lens of

$$R = -\frac{g}{N}\frac{\tan\theta}{2}. \tag{5}$$

This radius of curvature can then be used to calculate the focal length of the latter lens *via*

$$f_{\rm lens} = -R/\delta. \tag{6}$$

With a parabolic material distribution the transmission function of the SRL is of Gaussian shape, as it also is for optimized CRLs with lenses of parabolic profile as described by Lengeler *et al.* (1999).

In this chapter the transmission function will be truncated such that the maximum optical path of the external ray in absorbing material is identical to the attenuation length (AL) of the lens material. This limits the length of the grooved structure L to $L = 2\,\mathrm{AL}$. The corresponding geometrical aperture of the lens is

$$2g = 2(2\delta\mathrm{AL})^{1/2} f^{1/2}. \tag{7}$$

Then the groove depth d respects $d = g$, which will be referred to in this study as the groove depth matching; and the corresponding geometrical aperture will be referred to as the aperture for optimum flux collection, as it already collects 84% of the transmittable flux.

For comparison purposes Fig. 2 now presents the lens gap $2g$ from (7) for a focal length of $f = 1$ m, and the lens length $L = 2\,\mathrm{AL}$ for some materials which have been used for the production of SRLs, namely Be, Si (Cederström *et al.*, 2000, 2001*b*, 2002*a*,*b*), Li (Dufresne *et al.*, 2001) and PMMA (polymethylmethacrylate, also referred to as plexiglass, *i.e.* $C_5H_8O_2$ with density 1.19 g cm^{-3}) (Jark, 2004). Both data for PMMA, which is a photoresist, are characteristic of other plastics which have very similar composition and density, like epoxies used by Cederström *et al.* (2002*a*,*b*) and polyvinyl chloride used by Kunimura & Kawai (2009). The same materials were also used for the production of CRLs (epoxies: Dudchik & Kolchevsky, 1999; Li: Cremer *et al.*, 2003; Si: Schroer *et al.*, 2003; Be: Lengeler *et al.*, 2004) as was Al (Lengeler *et al.*, 1999). The data are for photon energies below 100 keV and are based on the material properties from the database of Chantler *et al.* (2005). One sees that a correlation exists between the atomic number Z of the material, the maximum aperture and the related operation energy. Best performance is provided by low-Z materials (Li and Be) at smaller photon energy around and below 10 keV. On the other hand, towards larger photon energies ($E > 30$ keV) the apertures become similar and independent of Z as the beam attenuation will ultimately be limited by Compton scattering (James, 1967; Lengeler *et al.*, 1999). The largest apertures are then provided by rather long lenses of low-Z material. In this respect SRLs in Li (Dufresne *et al.*, 2001) will mostly be inconveniently long with lengths in excess of $L = 100$ mm. Towards larger photon energies materials with larger Z offer the advantage of rather short lens lengths below 100 mm. Plastics are then a convenient compromise material for the production of X-ray lenses for large tuning ranges.

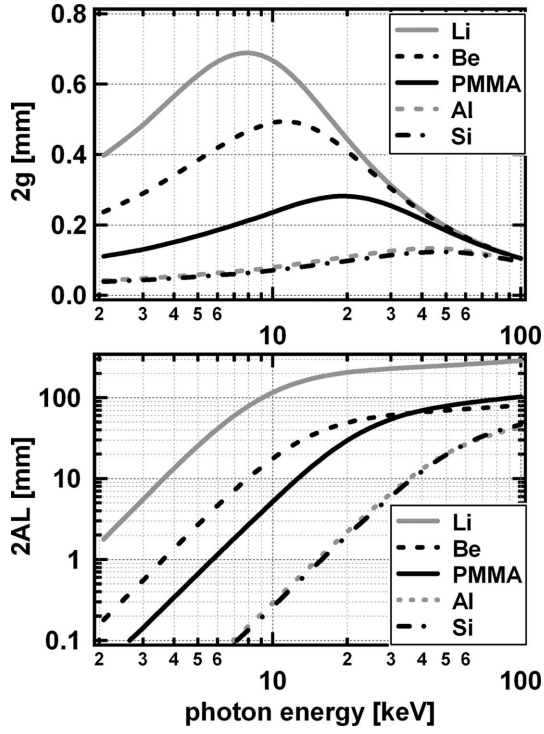

Figure 2
Dependence on photon energy of the lens gap $2g$ in SRLs with focal length of $f = 1$ m according to (7) (top) and of the optimum lens length 2AL (bottom), where AL is the attenuation length of the materials, for lighter materials, which were used in transmission lenses for X-rays, *i.e.* lithium (Li), beryllium (Be), plexiglass (PMMA), aluminium (Al) and silicon (Si).

The following discussion will be limited to the easier to handle materials Be, PMMA and Si, for which production strategies for SRLs have already been developed by Cederström *et al.* (2001*a*, 2002*a*,*b*). Grooved structures of high quality can also be produced in Si by anisotropic etching (Cederström *et al.*, 2002*a*). Such devices have then been used directly as X-ray lenses and they have been used for transferring the structure by embossing into Be and into epoxies (Cederström *et al.*, 2002*a*; Ribbing *et al.*, 2003*a*) and as master dyes for the chemical vapor deposition of diamond (Ribbing *et al.*, 2003*b*).

2.2. The optical path difference in SRLs

It will now be investigated whether the X-rays passing an SRL will respect basic optical principles. Fermat's principle requires for an ideally focusing optics that all possible optical paths between the source and the image are identical. Diffraction-limited operation requires the variation in the optical paths to respect the Rayleigh quarter-wavelength criterion (Born & Wolf, 1980). As the apertures of refractive X-ray lenses are small (<1 mm) compared with the distance to the synchrotron radiation sources (>10 m), throughout this study a plane incident wave is considered, which travels in Fig. 1 from left to right. The variation of the optical path (OP), *i.e.* the optical path difference (OPD), will be considered with respect to the on-axis optical path, which is the distance of the observation plane from the upstream termination of the lens.

The optical path in material is obtained *via*

$$\mathrm{OP}_{\mathrm{mat}} = nP(y) = (1-\delta)P(y) = P(y) - \delta P(y). \qquad (8)$$

Now, in general in refractive X-ray lenses the lens aperture is also small compared with the focal length of the lens. Then the paraxial approximation can be applied to all ray trajectories. When the thin-lens approximation is used, *i.e.* the finite lens thickness is ignored, it can easily be shown that the optical path difference cancels in lenses, in which the material distribution function $P(y)$ is of parabolic shape, the shape proposed by Lengeler *et al.* (1998).

2.2.1. Originally proposed orientation for the SRL. Evans-Lutterodt *et al.* (2003) challenged the validity of the thin-lens approximation for refractive X-ray lenses. They showed that the material distribution function $P(y)$ for a real 'thick' plane concave lens needs to be of elliptical shape in order to focus X-rays aberration-free. Then towards the lens border the material distribution function is steeper than in a parabolic lens leading to reduced transmission in this area. Now the SRL in Fig. 1 is even 'thicker', *i.e.* the refracting interfaces extend more towards the focus than the corresponding interface in a single elliptical lens. It is thus obvious that the parabolic material distribution in SRLs cannot direct all transmitted rays to a common crossover point in the focal plane. Thus

focusing using such a lens will suffer from aberrations in the image plane.

This study will first consider the lens orientation in Fig. 1, as was originally proposed by Cederström *et al.* (2000) and used in all their studies. The internal path in the lens will be separated into the paths OP_{mat} and OP_{gap}, which define the paths in material and in the free space between the prisms, respectively. The optical path difference in the SRL is then given by

$$\mathrm{OPD} = \mathrm{OP}_{mat}(y) + \mathrm{OP}_{gap}(y) + \mathrm{OP}_{free}(y) - f, \qquad (9)$$

where $\mathrm{OP}_{free}(y)$ is the optical path between the exit point from the SRL and the focal plane, *i.e.*

$$\mathrm{OP}_{free} = \left\{[f - E(y)]^2 + y^2\right\}^{1/2}, \qquad (10)$$

where $E(y)$ describes the exit point distance in the beam direction from the first prism tip.

In Appendix *A* the OPD according to (9) is derived considering all possible refraction processes, which lead to a curved beam trajectory in the lens. Surprisingly the resultant OPD is made up of only two terms,

$$\mathrm{OPD}_{orig} \simeq -\left(\frac{m}{N}\right)^2(\delta \mathrm{AL})\frac{\Delta f}{f} + \frac{4}{3}\left(\frac{m}{N}\right)^3(\delta \mathrm{AL})\left(\frac{\mathrm{AL}}{f}\right), \qquad (11)$$

where Δf is introduced for the distance of an observation plane from the nominal focal plane, and m refers to the prism tip index as shown in Fig. 1.

Interestingly, the latter equation contains exclusive material properties (δ and AL) and the focal length, but no parameter related to the exact shape of the prisms. The two terms vary with different power of m and it is thus impossible to find an observation plane with $\mathrm{OPD}_{orig} = 0$ for all m. Instead, the observation plane with minimum variation for the OPD can be determined.

Now the number M will be used in order to describe the use of a smaller than optimum aperture, *i.e.* $M < N$. In any case the minimum variation for the OPD is found when $\mathrm{OPD}(M) = 0$ is used for the limiting ray, which requires

$$\Delta f_{diff} = \frac{4}{3}\left(\frac{M}{N}\right)\mathrm{AL}. \qquad (12)$$

In this condition the maximum in the OPD is then found for $m/N = (2/3)(M/N)$, when it is

$$\mathrm{OPD}_{orig,min} = -\frac{16}{81}(\delta \mathrm{AL})\left(\frac{\mathrm{AL}}{f}\right)\left(\frac{M}{N}\right)^3. \qquad (13)$$

For diffraction-limited operation this variation needs to remain within the Rayleigh quarter-wave criterion; one can now derive the corresponding minimum focal length $f_{SRL,orig,min}$. It is given by

$$f_{orig,min} = \frac{64}{81}(\delta \mathrm{AL})\left(\frac{\mathrm{AL}}{\lambda}\right)\left(\frac{M}{N}\right)^3. \qquad (14)$$

The question to ask now is obviously whether the diffraction-limited spatial resolution obtained at this minimum focal length has any special significance. The diffraction-limited resolution depends in a complicated way on the choice of the resolution criterion, the lens transmission function and an eventual truncation of the latter owing to the use of beam-limiting apertures. For the ease of this presentation and in order to keep the discussion rather generally applicable the commonly found form for the diffraction-limited resolution employing spatially coherent radiation will be used here under all conditions (Born & Wolf, 1980),

$$s = 1.22\frac{\lambda}{2\mathrm{NA}}, \qquad (15)$$

where NA is the numerical aperture of the lens. It is essentially the prefactor, which can be reduced slightly to below 1.22 by appropriate choice of the transmission function, its truncation and the spatial coherence of the beam as discussed by Lengeler *et al.* (1999). At this point only a single structure forming a half-lens will be considered. The illumination will always be assumed to include the ray passing the single prism tip, and the numerical aperture as given by the geometrical aperture is then

$$2\mathrm{NA} = \frac{M}{N}\frac{g}{f}. \qquad (16)$$

By use of (7) one obtains

$$s = 1.22\frac{\lambda}{(2\delta \mathrm{AL})^{1/2}}\, f^{1/2}\, \frac{N}{M}. \qquad (17)$$

The spatial resolution s_{diff} corresponding to the minimum focal length from (14) is then

$$s_{diff} = 0.76(\lambda\, \mathrm{AL})^{1/2}\,(M/N)^{1/2}. \qquad (18)$$

At shorter focal length for an incident plane wave the OPD exceeds the Rayleigh quarter-wave criterion. Consequently then the focus is the result of increasingly incoherent interaction in the transmitted wavefield. In this case the intensity distribution can be predicted by use of ray-tracing calculations. This will be done here as much as possible analytically. In a given image plane at distance $f + \Delta f$ the rays then have an off-axis distance y_{focus}, which depends on the index of the prism from which they exit,

$$y_{focus} = \left[E(y) - \Delta f\right]\frac{y}{f} = 2\left(\frac{m}{N}\right)^2 \mathrm{AL}\,\frac{g}{f} - \Delta f\frac{m}{N}\frac{g}{f}. \qquad (19)$$

These two terms also vary with different smaller powers of m and thus a common intersection point for all rays will not be found. However, the extent of the smallest blurred image can be determined. For this purpose the absorption losses in the transmission process will be taken into account and any ray will be assigned the intensity with which it leaves the last prism. Then the full width at half-maximum (FWHM) spot size s_{ab} will be taken as the beam width, which contains 75% of the transmitted intensity. For the discussed aperture limitation a linear correlation is found between the so-determined FWHM spot size and the off-axis distance y of the border ray ($M = N$) in the nominal focal plane ($\Delta f = 0$). More generally, in a finite aperture ($< g$) according to (19) the border ray, *i.e.* the most aberrated ray, has $y_{focus}(\Delta f = 0) = 2(M/N)^2\mathrm{AL}(g/f)$. Here, in

the interesting image plane according to (12), one finds then for the aberrations-limited spot size,

$$s_{\rm ab} = 0.6\left[1 - 0.27(M/N)^2\right] y_{\rm focus}, \quad (20)$$

and thus

$$s_{\rm ab} = 0.6\left[1 - 0.27(M/N)^2\right](M/N)^2\,{\rm AL}(2\delta{\rm AL})^{1/2} f^{-1/2}. \quad (21)$$

By use of (14) the aberrations-limited spot size is then obtained as

$$s_{\rm ab} = 0.96\left[1 - 0.27(M/N)^2\right](\lambda{\rm AL})^{1/2}\,(M/N)^{1/2}. \quad (22)$$

This equation contains the same terms found in (18) and a numerical prefactor, which for $0 < M < N$ varies rather little from 0.96 to 0.70 for $M = N$. Both equations, (18) for diffraction-limited operation and (22) for the spot size blurring caused by aberrations, predict thus essentially the same spot size at the focal length for diffraction-limited operation. Now according to (21) the blurred spot size increases towards smaller focal length with $s_{\rm ab} \propto f^{-1/2}$ and starts to dominate the focus size.

Obviously the aberrations in (22) can be reduced by closing down an aperture in front of the lens, limiting this way the illumination to prisms with indexes $M < N$. Then according to (14) this will allow for diffraction-limited operation at significantly shorter focal length. We then ask what the special meaning of the focal length according to (14) is. It can easily be shown that this focal length provides the highest flux density. This contrasts with the finding in CRLs for one-dimensional focusing with parabolic transmission function, in which the flux density in the diffraction-limited focus size is independent of the focal length. Consequently, caused by the aberrations at shorter focal lengths with $f < f_{\rm orig,min}$, the SRLs will provide smaller flux density and eventually larger foci than CRLs, even though their transmission functions are identical!

As far as the aberrations are concerned one has to recognize that these aberrations can be lowered to 75% of the indicated number in a slightly different observation plane,

$$\Delta f_{\rm ab} = (3/2)(M/N){\rm AL} = \Delta f_{\rm diff} + (1/6)(M/N){\rm AL}. \quad (23)$$

Fig. 3 now presents for depth-matched lenses ($M = N$) the focal length $f_{\rm orig,min}$ according to (14) and the related minimum spatial resolution $s_{\rm diff}$ according to (18) depending on photon energy for the more promising materials Be, PMMA and Si with the material properties according to Chantler *et al.* (2005). We see that regular SRLs in Si will provide the more interesting aspect of diffraction-limited spatial resolution down to rather small focal length in the millimetre and centimetre range at smaller photon energies below about 30 keV. The corresponding spot sizes are of the order of 0.1–0.3 μm, *e.g.* a regular SRL in Si for a photon energy of 20 keV can provide a diffraction-limited spot size of 0.19 μm for a focal length $f = 16$ mm in a lens with a groove depth $d = 6.5$ μm and a lens length of only 2 mm. According to Fig. 2 at lower photon energies lenses in Be and PMMA provide larger apertures than lenses in Si. As far as the diffraction-limited spot size is concerned such lenses without aberrations could

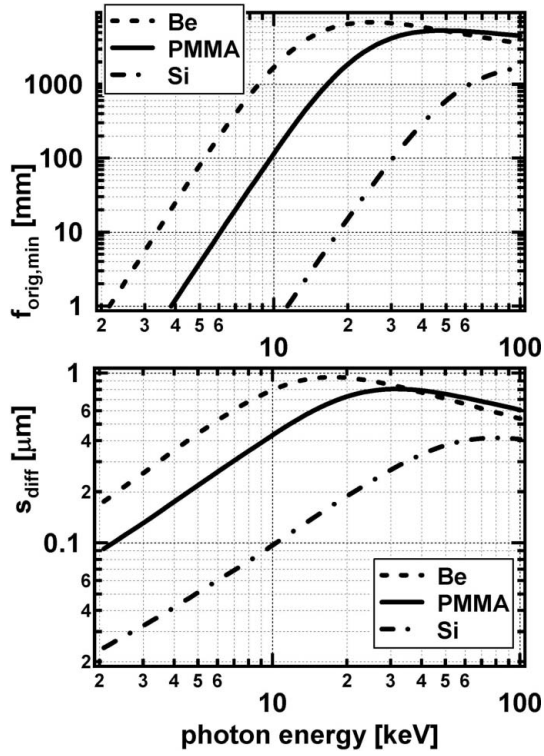

Figure 3
Dependence on photon energy of the minimum focal length for diffraction-limited focusing $f_{\rm orig,min}$ in SRLs according to (14) (top) and of the related diffraction-limited spot size $s_{\rm diff}$ according to (18) (bottom) for lenses in Be, PMMA and Si.

easily outperform the Si lenses even with longer focal lengths. Instead, with aberrations a similar spot size is out of reach at this photon energy for lenses in these materials, even when one closes an aperture in front of the lens in order to reduce the aberrations. By sacrificing half of the photon flux using $M = N/2$, according to (14) one would provide diffraction-limited operation at eightfold shorter focal length. However, according to (18) such an aperture closure will reduce the spot size only moderately to 0.7 of the diffraction-limited spot size for the depth-matched lens with optimum flux collection. Then for 20 keV photon energy an SRL in PMMA would provide $s_{\rm diff} = 0.5$ μm for a focal length of 0.25 m and, for a Be lens, $s_{\rm diff} = 0.7$ μm for $f = 0.8$ m.

2.2.2. Reversed LP lens orientation. The above discussion cannot readily be applied to the lens when operated with reversed inclination, *i.e.* when the lens in Fig. 1 is flipped horizontally. Jark (2004), Shastri *et al.* (2007) and Said & Shastri (2010) used this lens orientation, which one would favour for a better dissipation of the power load in high-intensity beams. In this reversed configuration the first prism facing the incident beam will then no longer be subject to the entire load.

Now all exit points are in the last prism, and thus they are roughly at the same position upstream of the focus. Will this favourably affect the OPD? It can be shown that the parabolic material distribution as given in (4) will lead to a cancellation of the OPD when one assumes a straight path internal in the lens. Thus in this orientation the resultant OPD will be

produced only by a curved path. Now a ray on a curved path finds less material on its path than a hypothetical straight ray entering the lens at the same position. The OP and the OPD can be discussed with the strategy presented in Appendix *A*.

Owing to the internal curved path any ray leaves the lens displaced already towards the optical axis by Δy as given in Appendix *A* by (59). In this case the optical path downstream of the exit point is given by

$$\mathrm{OP}_{\mathrm{free}} = \left[(f + \Delta f)^2 + \left(\frac{m}{N} g - \Delta y \right)^2 \right]^{1/2}. \qquad (24)$$

Finally the OPD in the reversed lens is obtained as

$$\mathrm{OPD}_{\mathrm{curve,rev}} = -\left(\frac{m}{N}\right)^2 \delta \mathrm{AL} \frac{\Delta f}{f} - \frac{2}{3} \delta \mathrm{AL} \frac{AL}{f} \left(\frac{m}{N}\right)^3. \qquad (25)$$

Compared with (11) the second term now has a negative sign and is of half the magnitude. For depth-matched operation this requires then a negative correction factor $\Delta f_{\mathrm{diff,rev}} = -(2/3)\mathrm{AL}$ for the minimum variation. The focal length for diffraction-limited operation $f_{\mathrm{rev,min}}$ is then twofold shorter. At this point the spot size is reduced to 70% of the previous result. In aberrations-limited operation the smallest spot is then found rather far away for $\Delta f_{\mathrm{ab,rev}} = \Delta f_{\mathrm{diff,rev}} - (5/6)\mathrm{AL}$, where the spot size blurring is found to be twofold smaller than in the original lens orientation. In this orientation the focusing is thus less affected by aberrations; nevertheless, the spot size blurring remains substantial.

2.3. SRL operation away from the boundary conditions

The theoretical treatment up to this point is rigidly connected to the depth-matching. A real lens, on the other hand, has a fixed groove depth *d*. The matching is then achieved for particular working curves of focal length *f* and photon energy, which can be derived from (7),

$$f_{d=g} = \frac{d^2}{2\delta \mathrm{AL}}. \qquad (26)$$

The tuning option of the SRL concept will more likely be used for the focusing of varying photons energies into a fixed image plane, and eventually for zooming the focus position at fixed photon energy. Then, in order to predict the effect of the aberrations under real experimental conditions, some modifications need to be applied to the previous findings. For a given *d* and for a particular photon energy or wavelength, *i.e.* for a set of values for δ and AL, one can determine $f_{d=g}$ using (26). The corresponding spot size limited by diffraction is simply estimated by

$$s_{\mathrm{diff}}(f_{d=g}) = 1.22\lambda(f/d). \qquad (27)$$

Instead, the size of the aberrations-limited spot in the original lens orientation is given by

$$s_{\mathrm{ab}}(f_{d=g}) = 0.33\,\mathrm{AL}(d/f), \qquad (28)$$

while it is about twofold smaller in the reversed lens orientation.

When this lens is now operated at $f > f_{d=g}$ the effectively refracting lens aperture will remain fixed at *d*. Instead, for $f < f_{d=g}$ the aperture varies according to $d > g \propto f^{1/2}$. By use of (15) and (16) one finds for the diffraction-limited spot size $s_{\mathrm{diff}} \propto (f/g)$. This latter size depends then on the focal length in the following way,

$$\begin{aligned} s_{\mathrm{diff}}(f < f_{d=g}) &\propto f^{1/2} \quad \text{and} \\ s_{\mathrm{diff}}(f > f_{d=g}) &\propto f. \end{aligned} \qquad (29)$$

The aberrations-limited spot size was found to be correlated to the off-axis position of the most aberrated ray in the nominal focal plane, and thus varies in the original orientation according to $s_{\mathrm{ab}} \propto E(y = g)(g/f)$, where $E(y = g)$ is the distance between the lens entrance and the prism tip, from which the outermost ray exits the SRL. Now, in a lens with fixed tip periodicity the latter distance varies as $E(y = d) \propto (1/f)$ and $E(y = g) \propto f^{-1/2}$. Consequently one finds the variations

$$\begin{aligned} s_{\mathrm{ab}}(f < f_{d=g}) &\propto 1/f \quad \text{and} \\ s_{\mathrm{ab}}(f > f_{d=g}) &\propto 1/f^2. \end{aligned} \qquad (30)$$

2.4. Operation of full SRL

SRLs are always drawn with two touching tips by Cederström *et al.*, who consider this orientation with the rotation axis in the touching point to be important (Cederström, 2001*a*). In the present treatment the intensity distributions in the observation planes for diffraction-limited operation and for minimum aberrations have a narrow peak with a significant tail extending essentially to only one side. Most of the intensity is refracted to beyond the optical axis, while the tail with reduced intensity crosses it. This requires the two lens halves to be separated when the smallest spot size is to be obtained with the best overlap of the intensity distributions. This separation then varies in a complex way with the focal length, the photon energy and the lens illumination. Consequently, when a tuning at the smallest spot size is projected, more motions than just a simple half-lens rotation are required. Rather generally it can be stated that the diffraction-limited spot size in the focal plane for minimum OPD for a full lens with touching tips at the lens termination will not improve beyond the spot size obtainable by use of a half-lens. However, the flux as well as the flux density will increase twofold.

3. Discussion

3.1. Interpretation of existing experimental data

The suitability of SRLs for microfocusing was studied by Cederström *et al.* (2002*a*,*b*), by Ribbing *et al.* (2003*a*,*b*) and by Shastri *et al.* (2007) for single-lens elements and for full lenses. The reported lenses all have groove depths of 0.1 mm. This choice is driven by the space available in clinical mammography instrumentation between the X-ray source and the detector. Usually a distance of around 1 m is chosen, which requires then for the refocusing an optical component with at

least fourfold smaller focal length, *i.e.* $f < 0.25$ m. If now an SRL, prepared either in Be or in epoxy, is to refocus the source onto the detector for photon energies of around 20 keV, as discussed by Fredenberg *et al.* (2008), according to equation (7) it will optimally collect the photon flux with groove depths of about 0.1 mm. The Si lens with the same depth, *i.e.* the master dye for the production of the epoxy lenses, instead is depth-matched in the photon energy range 20–100 keV for rather long focal lengths 2.6 m $< f <$ 4.5 m, which are always larger than the minimum focal length for diffraction-limited operation. In the latest study by Shastri *et al.* (2007) such a Si lens was used at a rather high photon energy of 81 keV. It is not yet depth-matched; however, with a focal length of $f = 1.27$ m it is operated above the minimum focal length for diffraction-limited operation in the reversed orientation of $f_{\rm rev,min} = 0.73$ m. Shastri *et al.* (2007) carefully aligned both lens halves independently for coinciding foci, and thus the diffraction-limited spot size should have been significantly smaller than the expected demagnified source size of 0.5 µm. Consequently lens internal aberrations cannot explain the large measured spot size of 2 µm, which Shastri *et al.* (2007) explain with defects in the beam transport and distortions introduced by the lens holder.

Shastri *et al.* (2007) and Said & Shastri (2010) tested Si lenses also for long-focal-length focusing and as X-ray beam collimators. In both applications the focal lengths by far exceeded the focal length for diffraction-limited operation $f_{\rm orig,min}$ according to (14) as presented in Fig. 3. It can be observed rather generally that $f_{\rm orig,min}$ is smaller than the focal lengths, which are needed for X-ray collimators at synchrotron radiation sources. Consequently regular saw-tooth refractive lenses can be used for this purpose. However, one has to make sure that more than two prisms are illuminated in such a lens. Otherwise the device would act as an interferometer, as described by Isakovic *et al.* (2010). This latter situation will be encountered when the base length in a prism of height g/N exceeds the attenuation length AL of the material. From the geometry and from (5) and (6) one can then formally derive the focal length f_2, which is not to be exceeded, as

$$f_2 \leq \frac{\mathrm{AL}\tan^2\theta}{4\delta}. \qquad (31)$$

This focal length increases very rapidly towards larger photon energy. However, at 10 keV photon energy it can be as small as $f_2 = 13.5$ m for the Si SRL presented by Shastri *et al.* (2007). It will be even smaller for shallower prisms.

The first four studies deal with lower X-ray energies between 14 keV and 30 keV and SRLs in the originally proposed orientation. The experiments were performed at the synchrotron radiation beamline BM05 (http://www.esrf.eu/UsersAndScience/Experiments/Imaging/BM05/) at ESRF at a source distance of $q = 40$ m and with focal lengths varying between 0.25 m and 0.61 m. In this case the vertical source size was of the order of $s_{\rm source} = 80$ µm, and thus the size of the demagnified source image, $s_{\rm image} = s_{\rm source}(f/q)$, is expected in the interval 0.5 µm $< s_{\rm image} <$ 1.25 µm. Single-grooved structures as well as full SRLs were tested. Cederström *et al.* (2001*a*, 2002*a*) pre-aligned the full lenses with touching tips by use of microscopes. They estimated that the procedure succeeded to achieve the touching to within a few micrometres. As the latter uncertainty cannot be ignored compared with the expected image size, the tests at these objects can only be used to a limited extent for the verification of the presented ideas. The tests at the single lenses instead can be used for this purpose. All experimental data are presented as filled circles in Figs. 4 and 5. The measurements are compared with the expectations depending on the focal length for the demagnified source size (solid black line), the diffraction-limited spot size (dashed line) and the spot size including also the aberrations (grey line). The latter estimates follow the considerations in §2.3. and the convolution is made by use of

$$S = \left(s_{\rm diff}^2 + s_{\rm abb}^2\right)^{1/2}. \qquad (32)$$

Symbols indicate the minimum focal length for diffraction-limited operation according to (14) (open square) and the focal length for depth-matching according to (26) (open diamond) with the related diffraction-limited spot sizes. The experimental data for lenses in epoxy are compared with the

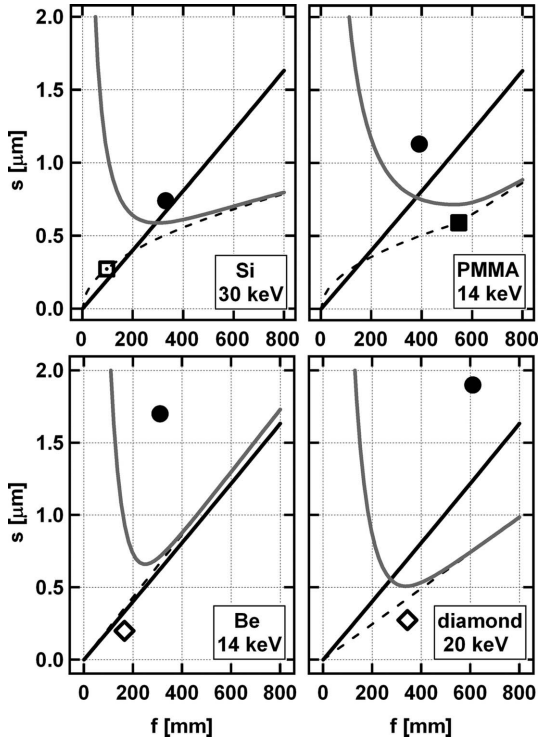

Figure 4
Comparison between measured spot sizes (filled circles) and the expectations (lines) depending on the focal length for single structures in different materials. The inclined solid line crossing the origin is the expected demagnified source size $s_{\rm image}$. The dashed line is the expected diffraction-limited spot size and the grey line is the expected spot size owing to aberrations and diffraction. Open squares present the focal length and the expected spot size for diffraction-limited focusing according to (14) and (18). Diamonds show the focal length and the related diffraction-limited spot size for depth-matched focusing according to (26) and (27). Both focal lengths coincide in filled squares.

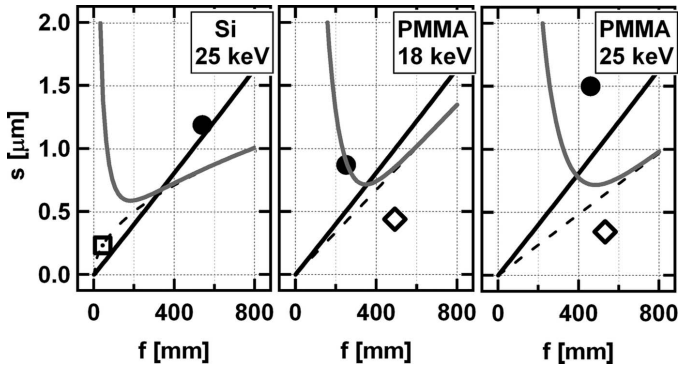

Figure 5
Comparison between measured spot sizes (filled circles) and the expectations (lines) depending on the focal length for full lens structures in different materials. For the explanation of the symbols and the lines see caption for Fig. 4.

expectations for the material properties of the plastic PMMA, which is expected to have similar composition and density.

The best performance is expected for the lenses with the best tip quality, *i.e.* for those etched into Si and for those replicated by punching the latter into epoxy. The single lens in Si provided at 30 keV almost source-size-limited operation. The measured spot size of 0.74 mm is the smallest spot size obtained up to now by use of SRLs. According to the present study the diffraction and the aberrations would limit the obtainable spot size in this case to the only slightly smaller value of about 0.6 μm. The chosen focal length was optimal for the lens parameters. One has to note, however, that this lens is operated far from depth-matching with $g < d$. Thus the lens extent into the direction of the focus is significantly larger than the optimum length. For this reason the aberrations dominate the spot size at the indicated focal length for diffraction-limited operation, which is significantly smaller than the chosen focal length. By use of a depth-matched lens a spot size of the order of 0.25 μm would then have been possible for $f = 100$ mm.

For the single replicated lens in epoxy and for a photon energy of 14 keV one now finds that the focal length for depth-matching and for diffraction-limited operation coincide with $f_{\rm orig,min} = f_{d=g} = 540$ mm. With this focal length a diffraction-limited spot size of the order of 0.7 μm should have been possible; however, the source size limited the expectation for this focal length to a spot size of about 1.2 μm. In the experiment a similar spot size was observed for the shorter focal length of $f = 390$ mm. According to the present study this focal length should have provided the smallest spot size in the chosen geometry.

It was known that the single lens in Be had a bowed surface as a result of the production process. Likewise the diamond lens had a wavy surface. Both defects will introduce aberrations, which were minimized by closing an aperture in front of the lenses. In the case of Be the closure was to half of the groove depth. The result of such a closure can be predicted very easily. It will double the diffraction-limited spot size at the groove-depth-matched focal length $f_{d=g}$, while it will reduce fourfold the blurring owing to aberrations. Then the optimum lens aperture g will be matched to the reduced aperture A at a fourfold-smaller focal length. This latter focal length is then the new reference point below which the dependence of the diffraction-limited spot on focal length will change from f to $f^{1/2}$. Likewise the dependence of the aberrations on focal length will change from $1/f^2$ to $1/f$. For these lenses the diamonds indicate the focal length for the depth-matching with the real groove depth. The spot size blurring owing to aberrations and to diffraction instead are now computed for the reduced aperture. Then the diffraction-limited spot size and the demagnified source size coincide for the Be lens at 14 keV. Both distorted lenses provide larger spot sizes than expected. They are larger than the expected blurring owing to aberrations in perfect saw-tooth lenses and to diffraction. Consequently these spot sizes are limited by the remaining aberrations introduced by the distortions in the lens surfaces.

The performance of the full lenses is compared with the expectations for half lenses, which, according to the discussion in §2.4, predict also the spot size expected from full SRLs with touching tips at the lens termination. For the epoxy lenses the expectations take into account that the beam size limitation by use of an aperture with opening 0.1 mm, as positioned upstream of the lens, will restrict the illumination in the two facing saw-tooth structures to only half of the groove depth of 0.1 mm. All results are compatible with the expectations according to this study. The Si lens is operated at 25 keV in the diffraction-limited regime far from any blurring expected from the aberrations. The measured spot size coincides well with the expected demagnified source size. However, this was achieved for a rather large focal length and smaller foci should have been possible by use of shorter focal length.

The data for the full lenses in epoxy present the expected aberrations-limited spot size of 0.87 μm for 18 keV photon energy and a significantly larger spot size at 25 keV. Owing to the uncertainty in the alignment these results cannot be further discussed. However, it should be noted that the result for 18 keV will then require a very careful alignment of the lens optical axis into the centre of the aperture. Instead the excessively large spot in the experiment at 25 keV would also have been observed when the aperture would have accidentally illuminated only one of the lens halves over the entire depth. The latter misalignment would have introduced a significant blurring owing to increasing aberrations introduced by the outermost rays.

The simulations show that rather independently of the lens material and the chosen photon energy the aberrations in the SRLs would have limited the microfocusing to very similar spot sizes between about 0.5 μm and 0.7 μm. These sizes should mostly have been possible to achieve under the chosen experimental conditions. Consequently the aberrations interfere with the possibility of using the SRLs efficiently as focusing devices for high-spatial-resolution experiments at synchrotron radiation sources. At this point the flexibility of the SRL concept makes it highly desirable to study, whether the aberrations in these lenses can be reduced or eventually even be removed.

Here it should be recalled that the theoretical treatment as well as the data interpretation assumes incident plane waves. In laboratory experiments with much shorter distances the incident rays can be inclined rather significantly with respect to the optical axis of the lens. This will give rise to additional aberrations, which are not discussed here. Consequently the present findings cannot readily be applied for the micro-focusing in this condition. In the case of mammography configurations, as discussed by Fredenberg *et al.* (2008), the SRLs are operated as beam concentrators providing rather large spots, which are then not affected by the aberrations in regular SRLs.

3.2. Strategies for aberrations removal

The boundary conditions for the aberrations reduction are rather obvious. First of all the rays passing the extended lens all need to cross the optical axis at the same point. The OPD between them also needs to respect the Rayleigh quarter-wave criterion. The first point will require the rays to follow paths different from the paths with constant curvature in the lens. This can be achieved with different strategies; for example, the structure could be made aperiodic in beam direction. Such a scheme with constant prism tip angle is proposed by Cederström (2001*a*) in order to reduce the lens length, which can then be limited to the length of the equivalent plane-parabolic lens. Now according to Evans-Lutterodt *et al.* (2003) the latter shape does not respect Fermat's principle. Consequently some further correction will be needed.

Here another approach will be presented, in which the structure periodicity will be kept constant and all tips of a half lens will be kept in a common plane. This facilitates very much the theoretical treatment, which will also be limited to $\Delta f = 0$.

3.2.1. SRL in originally proposed orientation. For the original lens orientation the path curvature in the lens internal will initially be ignored. Then the off-axis rays need to accumulate a slowly increasing deflection angle on their path in order to be directed from their exit points to a common crossover point on the optical axis. The prisms will be approximated by planar objects. Then the requirement for the beam path can be written along the lens internal path approximately as

$$\left(\sum_{n=1}^{m}\Delta_n\right)\Big[f-(m-1)p\Big]=m(g/N). \tag{33}$$

The solution to this system of equations, which are applied recursively, is

$$\Delta_m=\Delta_1\,\frac{f}{f-(m-2)p}\,\frac{f+p}{f-(m-1)p}. \tag{34}$$

As far as the inclination of the prism side-walls is concerned, the related slope can then be simplified to

$$\tan\theta_m\simeq\tan\theta_1\left[1-(m-1)\,\frac{p}{f}\right]^2. \tag{35}$$

Interestingly, this modification no longer contains material properties but very generally only the lens focal length and the lens periodicity. Consequently the structure periodicity p can be chosen rather freely. Now the lens length minimization by depth-matching has lost its importance. Nevertheless, one has to limit the lens length to $L = Np < f$. The variation in the prism angle according to (35) will now lead to a variation of the groove depth. Consequently in the parameter optimization process it needs to be assured that the curved paths for all rays will always pass a gap between adjacent prisms. The respect of this boundary condition can be checked by ray-tracing calculations. Such calculations need to be employed in any case in order to account appropriately for the curved path and for the increasing inclination of the beam path in the gaps between the prisms and in the prisms. The rigorous ray-tracing calculations for an incident plane wave show that the variation in the OPD can be kept significantly below the Rayleigh quarter-wave limit when one introduces a correction factor c in (34), modifying it to

$$\tan\theta_m\simeq\tan\theta_1\left[1-c(m-1)\,\frac{p}{f}\right]^2. \tag{36}$$

This factor is only slightly larger than 1 and it compensates for all approximations made in the derivation of (35), namely for the straight path and the planar prism approximation. In SRLs with the prism angle variation given by (36) the aberrations are eliminated and consequently diffraction-limited operation for any focal length is then possible. However, unlike in the normal SRL, now the prism periodicity p has become an important parameter for the lens operation. This parameter and the ratio p/f now need to be kept fixed, and thus in an aberrations-corrected SRL one loses the focal length zooming capability. However, the practically more interesting photon energy tunability in a slit at fixed position is still maintained.

3.2.2. SRL in reversed orientation. In the lens in the reversed orientation one now has to intervene on the curved path in the lens for the following scope. Here the rays need to accumulate a slowly decreasing deflection angle in their path in order to be directed from the exit point, with accordingly corrected off-axis distance, to the common crossover point on the optical axis at distance f.

In the single prism one needs

$$\Delta_1 f=(g/N). \tag{37}$$

For the rays passing two prism tips this requires

$$\Delta_2(f+p)+\Delta_1 f=2(g/N)-\Delta_2 p, \tag{38}$$

and then

$$\Delta_3(f+2p)+\Delta_2(f+p)+\Delta_1 f=3(g/N)-\Delta_2 p-2\Delta_3 p. \tag{39}$$

More generally it requires

$$\sum_{n=1}^{m}\Delta_n\Big[f+(n-1)p\Big]=m(g/N)-\sum_{n=1}^{m-1}n\Delta_n p, \tag{40}$$

and the difference between adjacent rows is then

$$\Delta_m\Big[f+(m-1)p\Big]=(g/N)-(m-1)\Delta_m p, \tag{41}$$

which leads to

$$\Delta_m\left[1+2(m-1)\,\frac{p}{f}\right]=\Delta_1 \tag{42}$$

and thus

$$\tan\theta_m=\tan\theta_1\left[1+2(m-1)\,\frac{p}{f}\right]. \tag{43}$$

In this case the prism angle variation once more depends on the fixed ratio p/f; however, now the correction algorithm contains only a linear dependence on it. The correction factor now has the opposite sign compared with (35) and thus the lens length $L = Np$ has no special limitation in relation to the focal length f. Here the choice of the optimum groove depth is less of a problem, as the last groove on the beam trajectory is the shallowest; instead, the others are deeper. Also here a correction factor c' needs to be introduced in order to accommodate the finite prism thickness,

$$\tan\theta_m=\tan\theta_1\left[1+2c'(m-1)\,\frac{p}{f}\right]. \tag{44}$$

Then by use of (44), with c' just slightly larger than 1/2, the Rayleigh criterion can be fulfilled formally for focal lengths which are even smaller than the attenuation length AL of the material, and thus of the lens length L. In any case in this lens orientation the clear distance between the lens and the sample is identical to the nominal focal length.

The presented strategy for the aberrations removal resembles very much the adiabatic CRL concept introduced by Schroer & Lengeler (2005). Also in adiabatic CRLs any successive structure is tailored to the properties of the already refracted beam. This way the numerical aperture NA of the lens system, which is identical to the maximum beam deflection, can be made to exceed the critical angle $\theta_{\rm crit} = (2\delta)^{1/2}$ of the lens material. Schroer & Lengeler (2005) did not succeed in achieving this in a stack of identical nanofocusing lenses (Schroer *et al.*, 2003). Evans-Lutterodt *et al.* (2003) observe that a single lens, in which Fermat's principle is respected, can deflect the X-ray beam at most by the critical angle $\theta_{\rm crit} = (2\delta)^{1/2}$. Now the SRLs, which are aberrations-corrected with the present strategy, are formally still single lenses. On the other hand in the stacked prisms the deflection angle per interface, and thus per unit length, is successively increasing like in adiabatic CRLs. The question is, thus, whether the resultant beam deflection can then exceed the critical angle. The more promising candidates for the related check are the aberrations-corrected SRLs mounted in the reversed orientation, in which they can provide the shortest focal lengths. The ray-tracing calculations show that the critical angle remains the limit for the beam deflection, when the SRLs respect Fermat's principle. Thus, as far as the numerical aperture is concerned, the present lenses still behave like single lenses. It is not clear whether this finding can be generalized to any kind of aberrations-corrected SRL or whether something other than the present strategy will provide more promising results. Now by use of the present lens concept the ultimately achievable spatial resolution remains limited to approximately $(\lambda/2{\rm NA}) = \lambda/[2(2\delta)^{1/2}]$. In the hard X-ray range, where one finds $\delta \propto \lambda^2$, this is a constant. The most promising lens material according to Schroer *et al.* (2003) is diamond, for which a spot size of the order of 16 nm is then predicted as the ultimate spatial resolution limit for the present lenses, when the numerical aperture coincides with the critical angle. Instead, for Si one would expect about 20 nm. These spot sizes would be found at a distance in the millimetre range from the lens termination. Consequently the reversed SRL would provide a more convenient working distance than CRL lens stacks, in which a similar focus size would be observed as close as 20 µm from the lens termination (Schroer & Lengeler, 2005).

3.3. Production issues

We now have to ask, what is possible with state-of-the-art production processes? Of the already applied production techniques for the saw-teeth, *i.e.* milling into thin plates (Cederström *et al.*, 2000, 2001*b*), anisotropic etching into Si crystals (Cederström *et al.*, 2002*a*) and sawing by use of a diamond blade (Said & Shastri, 2010), only milling and sawing allow for the free choice and the variation of the prism angle. The most promising process, the anisotropic etching, instead can only produce fixed angles. Obviously for high-spatial-resolution focusing the prism tips need to be positioned to within a fraction of the projected focus size, *i.e.* fractions of a micrometre, to the correct position. This requirement in combination with the angle variation is by far beyond the capabilities of standard workshop tools, and it will require very severe interventions onto the sample carriage similar to systems which are used for ruling diffraction gratings (see, for example, Hutley, 1982).

Only microfabrication will be able to provide sufficient accuracy in the already available state-of-the-art instrumentation. Evans-Lutterodt *et al.* (2003) and Schroer *et al.* (2003) describe promising processes in which original masks of high quality are always sacrificed in the production process. Instead, lithography into photoresists will allow mass production as a single original mask can be replicated an unlimited number of times. This supposedly cheaper production technique is thus discussed here. PMMA is a possible photoresist candidate for the lens production and thus the curves for PMMA in Fig. 2 show the expectations for the aperture and for the lens length. In this case the mask could be produced by high-resolution e-beam writing, which allows sufficient positioning precision. Especially deep X-ray lithography as the final replication process will then allow a replication even into a significant depth of a resist layer in the range 1–2 mm, as was shown by Nazmov *et al.* (2004). Possible production strategies for the intermediate and the final processes are reported by Pantenburg & Mohr (2001), Nazmov *et al.* (2004) and Pérennès *et al.* (2005).

As these processes always involve replications of original masks, the fidelity for the shapes of edges may not be guaranteed in all steps of the process. The principal expected defects are then rounded sharp tips and filled shallow corners,

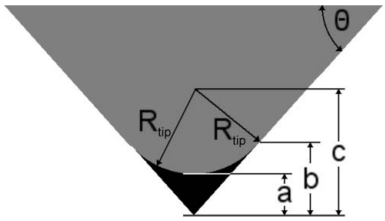

Figure 6
Geometric conditions in rounded prism tips (grey) with radius of curvature $R_{\rm tip}$. The rounding starts at a distance from the nominal tip position of $b + a$, where the straight side-wall is tangential to the rounded tip.

as discussed by Nazmov *et al.* (2004). Now in the SRL one has to be concerned only about the tips of the structures. A rounded tip will not refract the transmitted radiation into the correct direction. Efficient focusing will then require that the ray losses in the rounded tips will be small compared with the appropriately refracted photon flux. The geometrical conditions for this discussion are illustrated in Fig. 6.

In Fig. 6 the rays passing the zones indicated a and b will not be refracted appropriately to the focus. It will now be required that $a + b$ amounts to only 0.2 of the linear zone g/N in any prism. Then approximately 20% of the incident beam will be refracted inappropriately. This defect will then also introduce a periodic disturbance into the lens transmission function. As a result part of the misdeflected intensity will be contained in diffraction peaks with a separation given by

$$P = \frac{\lambda}{(g/N)}\, f. \tag{45}$$

It has already been shown for other structures based on prisms by De Caro & Jark (2008) that such a disturbance covering about 20% of the active area of the prism does not affect the diffraction-limited size of the primary focal spot, even though it reduces the flux into it. The parameter g/N can be derived from (5) and (6) and is

$$g/N = \frac{2f\delta}{\tan\theta}. \tag{46}$$

The geometry leads to

$$a + b = R_{\rm tip} \sin\theta \tan\theta \tag{47}$$

and the requirement then becomes

$$R_{\rm tip} = 0.4\,\frac{\delta f}{\sin\theta \tan^2\theta}. \tag{48}$$

Practically radii of curvature $R_{\rm tip}$ of the order of 1 µm are feasible by use of lithography (Nazmov *et al.*, 2004). According to (48) this is not compatible with close to rectangular prism tips and with shorter focal length. Consequently the prisms need to have smaller prism angles θ. In the small-angle approximation an estimate for the preferred prism angle leads to

$$\theta = \left(0.2\,\frac{2\delta f}{R_{\rm tip}}\right)^{1/3}. \tag{49}$$

An easily feasible example of the capabilities of deep X-ray lithography will be discussed here. According to Fig. 2 an SRL in PMMA or other plastic material starts to provide the best performance in terms of aperture at a photon energy of around 18 keV. Conservative numbers for the focal length f = 0.1 m and for the radius of curvature $R_{\rm tip} \simeq 2$ µm should then provide efficient focusing with a prism angle of about $\tan\theta \simeq \theta = 0.25$. Such an SRL would provide a diffraction-limited spatial resolution of $s_{\rm diff}$ = 0.1 µm = 100 nm with an optimum aperture of $2g$ = 0.08 mm, with $g/N \simeq 0.65$ µm and with N = 62 prisms in any lens half. The lens length is only about 22.5 mm. The indicated spatial resolution can then be achieved with aberrations-corrected SRLs in both orientations with structure periodicities of p = 0.36 mm. The correction factor, for example in (36), is then c = 1.03. The diffraction peak separation according to (45) is P = 10 µm. So the higher-order peaks can be eliminated by an appropriately positioned slit upstream of the focus position. This lens allows for a tuning of the photon energy in a fixed slit. In tuning to smaller photon energy, eventually to below 10 keV, no lens parameter will become critical; however, the spatial resolution will slowly increase. Towards larger photon energies, *i.e.* shorter wavelengths, the lens aperture hardly changes and thus diffraction-limited operation with spot sizes even below 100 nm is then possible according to (17). However, in this case g/N, as given in (46), will rapidly decrease towards larger photon energies owing to the rapid decrease of the refractive index decrement δ. Thus the limiting upper operation energy will depend on the realised tip radius $R_{\rm tip}$.

4. Alignment issues

A few tolerances are now important in the SRLs. First of all this regards the position of the prism tips in the half-lens, and secondly it regards the positioning of the two lens halves with respect to each other. The first will require the variation in g/N to be smaller than half the focus size. For the presented feasible example the prism tip positions then need to stay within 0.05 µm of the common plane containing the prism tips. This is possible to achieve with state-of-the-art instrumentation for the mask production.

Obviously the optical axes of both lens halves also need to be positioned with this tolerance with respect to each other. It can be shown that this tolerance then keeps the OPD for the whole lens aperture within the Rayleigh quarter-wave criterion. The latter tolerance is now smaller than the wavelength of visible light, which makes it an extremely demanding request, as it is out of reach for optical microscopes, which were used by Cederström (2001*a*) for aligning this degree of freedom. A more adapted in-operation alignment procedure thus needs to be developed.

The last question is, then, how well do the prism tips in both lens halves need to face each other? The OPD between the border ray and a ray on the optical axis needs to remain within the Rayleigh quarter-wave criterion. The optical path for the border ray is OP = $F + y^2/2F$. The permitted consequence for the variation of the focal length is then

$$\frac{\partial}{\partial F}\mathrm{OP}\,\Delta F = -\frac{y^2}{2F^2}\Delta F = \frac{\lambda}{4},$$

and thus

$$\Delta F = \frac{\lambda}{2}\frac{F^2}{g^2}. \tag{50}$$

For the example case this gives a tolerable longitudinal misalignment between the two lens halves of $\Delta F \simeq 0.2$ mm. In this case it is roughly half of the periodicity p of the prisms. Such a misalignment has been used already by Jark (2004) in order to avoid tip damage owing to possible tip touching. Obviously the alignment tolerances for all discussed aspects can be relaxed significantly when an SRL is to be operated at a laboratory source with significantly larger spot sizes, which was actually the case in the original experiment of Cederström *et al.* (2000) and in the studies reported by Jark (2004) and by Fredenberg *et al.* (2008).

For the designer of optical instrumentation some of the presented findings will offer some interesting flexibility. First of all in the crossed pair for bi-dimensional focusing both lenses could be operated with almost identical focal length by appropriately making use of both lens orientations. On the other hand, the focal length in the SRL in the reversed orientation can be rather short compared with its length. Then the focal lengths in a lens pair can be made significantly different. By use of such an astigmatically focusing pair an elliptical source could then eventually be focused to a round spot. Then it can be especially advantageous that the lens in the reversed orientation can provide a rather short focal length in comparison with its length. A crossed pair of aberrations-corrected SRLs could thus be a very versatile tuning device for the focusing of X-rays in one and in two dimensions. It could thus be an interesting complementary addition to the X-ray transfocator described by Snigirev *et al.* (2009).

5. Conclusion

It is shown that SRLs in low-Z material, when they are based on highly regular structures and are operated at synchrotron radiation sources, can provide at best a spatial resolution of the order of 0.5 µm, as the internal aberrations limit the obtainable spot size. This is especially the case when the lenses are operated with larger apertures for optimum photon flux collection. Previously measured spot sizes in the submicrometre range obtained with high-quality half lenses are found to have been limited by these aberrations. A possible solution for this problem is identified. Now by introducing a variation in the angle of the grooves along the lens the aberrations can be removed and the SRLs can be projected for diffraction-limited operation. The modified lenses will then lose the focal-length zooming option but they will keep the more interesting photon energy variation in a fixed slit. So the SRL remains a very flexible lens concept for diffraction-limited operation. It will perform essentially identically to CRLs of the same material with identical focal length for the same photon energy. However, it should be noted that the SRL remains a lens for one-dimensional focusing, for which it can provide high diffraction-limited spatial resolution ultimately to spot sizes as small as 14 nm. The aberrations correction is not needed when SRLs are projected for focusing to larger focus sizes at synchrotron radiation sources and also in combination with laboratory X-ray sources.

APPENDIX *A*
Derivation of the optical path difference in the SRL in the original orientation

Cederström *et al.* (2001*a*,*b*) have shown already that the optical path variation within any interval g/N (see Fig. 1), in which the material distribution varies linearly, is significantly smaller than a quarter-wavelength when compared with the ideal parabolic material distribution. This finding allows us to simplify the discussion by computing the optical path within any interval g/N for only one ray. Consequently one can then change from the continuous variable y to the integer variable m, which is the prism tip index. The corresponding paths are then

$$\mathrm{OP}_{\mathrm{mat}}(m) = n(m/N)^2\mathrm{AL} \tag{51}$$

and

$$\mathrm{OP}_{\mathrm{gap}}(m) = 2(m/N)\mathrm{AL} - (m/N)^2\mathrm{AL}. \tag{52}$$

The coordinates of the exit point are

$$E(m) = 2(m/N)\mathrm{AL} \tag{53}$$

and

$$y = (m/N)g. \tag{54}$$

This leads to

$$\begin{aligned}\mathrm{OP}_{\mathrm{mat}}(m) + \mathrm{OP}_{\mathrm{gap}}(m) &= \mathrm{OP}_{\mathrm{int}}(m)\\ &= 2(m/N)\mathrm{AL} - (m/N)^2(\delta\mathrm{AL}).\end{aligned} \tag{55}$$

For a more general consideration a variation in the detector plane position Δf will be permitted. This changes the optical path on the lens axis to

$$\mathrm{OP}_{\mathrm{centre}} = f + \Delta f$$

and for any other ray to

$$\mathrm{OP}_{\mathrm{free}} = \left\{[f + \Delta f - 2(m/N)\mathrm{AL}]^2 + [(m/N)g]^2\right\}^{1/2}, \tag{56}$$

to be applied in the paraxial approximation.

In the OPD formed according to (9) most of the terms cancel and only two are left for a supposedly straight path,

$$\mathrm{OPD}_{\mathrm{str}} \simeq -(m/N)^2(\delta\mathrm{AL})(\Delta f/f) + 2(m/N)^3(\delta\mathrm{AL})(\mathrm{AL}/f). \tag{57}$$

However, unlike in a single concave lens, in the SRL the rays undergo several deflection processes, which lead to a curved path in the lens internal. So a curvature correction needs to be applied to the straight path OP in (55) and thus to the OPD in (57). The deflection angle after passage through a single prism was derived by Cederström (2001*a*) as

$$\Delta\alpha = 2\delta/\tan\theta. \quad (58)$$

This angle is small and thus the resultant deflection angle behind m prisms is simply cumulative, *i.e.* it is $m\Delta\alpha$. Here the single prisms will be assumed to be planar objects. Then a deflected beam is vertically displaced between two prisms of separation p by $p\Delta\alpha$. Up to the prism with index m the beam accumulates the displacement for $m-1$ intervals, resulting in a total displacement towards the optical axis of the lens by

$$\Delta y_{\rm vert}(m) = \sum_{n=1}^{m-1} p\Delta\alpha n \simeq \frac{p\Delta\alpha}{2} m^2. \quad (59)$$

This leads to a curved lens internal path, in which the rays progress roughly on a circle with radius of curvature ρ given *via* $\Delta\alpha\rho = p$. In order to exit from the prism with index m then a ray needs to enter the prism array displaced by the corresponding $\Delta y_{\rm vert}(m)$ according to (59) further away from the optical axis. Compared with the straight path to the same exit point the curved internal path of the lens will now be longer and it will pass more material.

The increased inter-prism path length after the first deflection process is

$$\Delta p = p\left(1+\Delta\alpha^2\right)^{1/2}. \quad (60)$$

The total path increase along the lens internal path, compared with $(m-1)p$, and for small $\Delta\alpha$ is then approximately

$$\Delta{\rm OP}_{\rm int} = \sum_{n=1}^{m-1} n^2 \frac{p}{2}\Delta\alpha^2 \simeq \frac{p}{6}\Delta\alpha^2 m^3 = \frac{2p}{3}\frac{\delta^2}{\tan^2\theta} m^3. \quad (61)$$

As far as the path change in material is concerned, after a displacement by $p\Delta\alpha$ the path increase or decrease amounts to $p\Delta\alpha\Delta P(y)/\Delta y$, where $\Delta P(y)/\Delta y$ is the gradient in the material distribution of the single prisms. For triangular prisms one finds $\Delta P(y)/\Delta y = 2/\tan\theta$. The path change accumulates in $m-1$ intervals and it needs to be subtracted from the additional path for the straight ray passing the correspondingly higher entrance point.

This latter additional amount of material is simply given by

$$\Delta y_{\rm vert}\frac{2}{\tan\theta} m = \frac{p\Delta\alpha}{\tan\theta} m^3. \quad (62)$$

Thus the accumulated path change in material is given as

$$\Delta{\rm OP}_{\rm mat} = \frac{p\Delta\alpha}{\tan\theta} m^3 - \sum_{n=1}^{m-1} \Delta y_{\rm vert}\frac{2}{\tan\theta} = \frac{4p}{3}\frac{\delta}{\tan^2\theta} m^3. \quad (63)$$

For the present boundary conditions, *i.e.* for depth-matched SRLs, one has

$$p = L/N = 2{\rm AL}/N \quad (64)$$

and

$$\tan\theta = 2d/p = 2g/p = Ng/{\rm AL}. \quad (65)$$

Then (61) and (63) can be written as

$$\Delta{\rm OP}_{\rm int} = (2/3)(\delta{\rm AL})({\rm AL}/f)(m/N)^3, \quad (66)$$

$$\Delta{\rm OP}_{\rm mat} = (4/3){\rm AL}({\rm AL}/f)(m/N)^3. \quad (67)$$

The correction to be applied to (67) deals then with the latter additional path in material, the corresponding path reduction in the gap $\Delta{\rm OP}_{\rm gap} = -\Delta{\rm OP}_{\rm mat}$, and the overall internal path increase given by (66). The required correction value is then

$$n\Delta{\rm OP}_{\rm mat} - \Delta{\rm OP}_{\rm mat} + \Delta{\rm OP}_{\rm int} = -(2/3)(\delta{\rm AL})({\rm AL}/f)(m/N)^3. \quad (68)$$

This correction for the curved path will thus reduce the second term in (57) to two-thirds of its value, resulting in

$$\begin{aligned}{\rm OPD}_{\rm curve} \simeq\ & -(m/N)^2(\delta{\rm AL})(\Delta f/f) \\ & +(4/3)(m/N)^3(\delta{\rm AL})({\rm AL}/f). \end{aligned} \quad (69)$$

The project is supported by the EU within the I3 action: European Light Sources Activities (ELISA)

References

Born, M. & Wolf, E. (1980). *Principle of Optics*, 6th ed. Oxford: Pergamon Press.

Cederström, B. (2001*a*). PhD thesis, Royal Institute of Technology, Stockholm, Sweden.

Cederström, B., Cahn, R. N., Danielsson, M., Lundqvist, M. & Nygren, D. R. (2000). *Nature (London)*, **404**, 951.

Cederström, B., Danielsson, M. & Lundqvist, M. (2001*b*). *Proc. SPIE*, **4145**, 294–302.

Cederström, B., Lundqvist, M. & Ribbing, C. (2002*a*). *Appl. Phys. Lett.* **81**, 1399–1401.

Cederström, B., Ribbing, C. & Lundqvist, M. (2002*b*). *Proc. SPIE*, **4783**, 37–48.

Chantler, C. T., Olsen, K., Dragoset, R. A., Chang, J., Kishore, A. R., Kotochigova, S. A. & Zucker, D. S. (2005). *X-ray Form Factor, Attenuation and Scattering Tables* (Version 2.1). National Institute of Standards and Technology, Gaithersburg, MD, USA. Originally published as Chantler, C. T. (2000). *J. Phys. Chem. Ref. Data*, **29**, 597–1048; and Chantler, C. T. (1995). *J. Phys. Chem. Ref. Data*, **24**, 71–643.

Cremer, J. T., Piestrup, M. A., Beguiristain, H. R., Gary, C. K. & Pantell, R. H. (2003). *Rev. Sci. Instrum.* **74**, 2262–2266.

De Caro, L. & Jark, W. (2008). *J. Synchrotron Rad.* **15**, 176–184.

Dudchik, Yu. I. & Kolchevsky, N. N. (1999). *Nucl. Instrum. Methods Phys. Res. A*, **421**, 361–364.

Dufresne, E. M., Arms, D. A., Clarke, R., Pereira, N. R. & Dierker, S. B. (2001). *Appl. Phys. Lett.* **79**, 4085–4087.

Evans-Lutterodt, K., Ablett, J. M., Stein, A., Kao, C.-C., Tennant, D. M., Klemens, F., Taylor, A., Jacobsen, C., Gammel, P. L., Huggins, H., Ustin, S., Bogart, G. & Ocola, L. (2003). *Opt. Express*, **11**, 919–926.

Fredenberg, E., Cederström, B., Aslund, M., Ribbing, C. & Danielsson, M. (2008). *X-ray Opt. Instrum.*, **2008**, 635024.

Hutley, M. C. (1982). *Diffraction Gratings.* London: Academic Press.

Isakovic, A. F., Stein, A., Warren, J. B., Sandy, A. R., Narayanan, S., Sprung, M., Ablett, J. M., Siddons, D. P., Metzler, M. & Evans-Lutterodt, K. (2010). *J. Synchrotron Rad.* **17**, 451–455.

James, R. W. (1967). *The Optical Principles of the Diffraction of X-rays.* Ithaca: Cornell University Press.

Jark, W. (2004). *X-ray Spectrosc.* **33**, 455–461.

Kunimura, S. & Kawai, J. (2009). *Spectrochim. Acta B*, **64**, 771–774.

Lengeler, B., Schroer, C. G., Kuhlmann, M., Benner, B., Günzler, T. F., Kurapova, O., Somogyi, A., Snigirev, A. & Snigireva, I. (2004). *AIP Conf. Proc.* **705**, 748–751.

Lengeler, B., Schroer, C., Tümmler, J., Benner, B., Richwin, M., Snigirev, A., Snigireva, I. & Drakopoulos, M. (1999). *J. Synchrotron Rad.* **6**, 1153–1167.

Lengeler, B., Tümmler, J., Snigirev, A., Snigireva, I. & Raven, C. (1998). *J. Appl. Phys.* **84**, 5855–5861.
Nazmov, V., Shabel'nikov, L., Pantenburg, F.-J., Mohr, J., Reznikova, E., Snigirev, A., Snigireva, I., Kouznetsov, S. & DiMichiel, M. (2004). *Nucl. Instrum. Methods Phys. Res. B*, **217**, 409–416.
Pantenburg, F. J. & Mohr, J. (2001). *Nucl. Instrum. Methods Phys. Res. A*, **467–468**, 1269–1273.
Pérennès, F., Matteucci, M., Jark, W. & Marmiroli, B. (2005). *Microelectron. Eng.* **78–79**, 79–87.
Ribbing, C., Cederström, B. & Lundqvist, M. (2003*a*). *J. Micromech. Microeng.* **13**, 714–720.
Ribbing, C., Cederström, B. & Lundqvist, M. (2003*b*). *Diamond Relat. Mater.* **12**, 1793–1799.
Said, A. H. & Shastri, S. D. (2010). *J. Synchrotron Rad.* **17**, 425–427.
Schroer, C. G., Kuhlmann, M., Hunger, U. T., Günzler, T. F., Kurapova, O., Feste, S., Frehse, F., Lengeler, B., Drakopoulos, M., Somogyi, A., Simionovici, A. S., Snigirev, A., Snigireva, I., Schug, C. & Schröder, W. H. (2003). *Appl. Phys. Lett.* **82**, 1485–1487.
Schroer, C. G. & Lengeler, B. (2005). *Phys. Rev. Lett.* **94**, 054802.
Shastri, S. D., Almer, J., Ribbing, C. & Cederström, B. (2007). *J. Synchrotron Rad.* **14**, 204–211.
Snigirev, A., Kohn, V., Snigireva, I. & Lengeler, B. (1996). *Nature (London)*, **384**, 49–51.
Snigirev, A., Snigireva, I., Vaughan, G., Wright, J., Rossat, M., Bytchkov, A. & Curfs, C. (2009). *J. Phys. Conf. Ser.* **186**, 012073.
Tomie, T. (1994). Japanese Patent JP2526409 (B2) (18 February 1994). [See also German Patent DE19505433 (C2) and US Patent application US5594773 (A)].